Murine Joubert syndrome reveals Hedgehog signaling defects as a potential therapeutic target for nephronophthisis

Ann Marie Hynes[a], Rachel H. Giles[b], Shalabh Srivastava[a], Lorraine Eley[a], Jennifer Whitehead[a], Marina Danilenko[a], Shreya Raman[c], Gisela G. Slaats[b], John G. Colville[d], Henry Ajzenberg[b], Hester Y. Kroes[e], Peter E. Thelwall[d,f], Nicholas L. Simmons[g], Colin G. Miles[a,1], and John A. Sayer[a,1]

[a]Institute of Genetic Medicine, International Centre for Life, Newcastle University, Newcastle upon Tyne NE1 3BZ, United Kingdom; [b]Department of Nephrology and Hypertension, University Medical Center Utrecht, 3508 GA, Utrecht, The Netherlands; [c]Histopathology Department, Royal Victoria Infirmary, Newcastle upon Tyne National Health Service Foundation Trust Hospitals, Newcastle upon Tyne NE1 4LP, United Kingdom; [d]Newcastle Magnetic Resonance Centre, Campus for Ageing and Vitality, Newcastle University, Newcastle upon Tyne NE4 5PL, United Kingdom; [e]Department of Medical Genetics, University Medical Center Utrecht, 3508 AB, Utrecht, The Netherlands; [f]Institute of Cellular Medicine, Newcastle University, Newcastle upon Tyne NE2 4HH, United Kingdom; and [g]Institute of Cell and Molecular Biosciences, Newcastle University, Newcastle upon Tyne NE2 4HH, United Kingdom

Edited by Kathryn V. Anderson, Sloan-Kettering Institute, New York, NY, and approved May 28, 2014 (received for review December 2, 2013)

Nephronophthisis (NPHP) is the major cause of pediatric renal failure, yet the disease remains poorly understood, partly due to the lack of appropriate animal models. Joubert syndrome (JBTS) is an inherited ciliopathy giving rise to NPHP with cerebellar vermis aplasia and retinal degeneration. Among patients with JBTS and a cerebello-oculo-renal phenotype, mutations in *CEP290* (*NPHP6*) are the most common genetic lesion. We present a *Cep290* gene trap mouse model of JBTS that displays the kidney, eye, and brain abnormalities that define the syndrome. Mutant mice present with cystic kidney disease as neonates. Newborn kidneys contain normal amounts of lymphoid enhancer-binding factor 1 (Lef1) and transcription factor 1 (Tcf1) protein, indicating normal function of the Wnt signaling pathway; however, an increase in the protein Gli3 repressor reveals abnormal Hedgehog (Hh) signaling evident in newborn kidneys. Collecting duct cells from mutant mice have abnormal primary cilia and are unable to form spheroid structures in vitro. Treatment of mutant cells with the Hh agonist purmorphamine restored normal spheroid formation. Renal epithelial cells from a JBTS patient with *CEP290* mutations showed similar impairments to spheroid formation that could also be partially rescued by exogenous stimulation of Hh signaling. These data implicate abnormal Hh signaling as the cause of NPHP and suggest that Hh agonists may be exploited therapeutically.

Recent genetic advances have allowed positional cloning and identification of numerous Joubert syndrome (JBTS) genes including *CEP290* (alias *NPHP6*) (1, 2), which encodes nephrocystin-6, a centrosomal protein (3). Mutations in *CEP290* account for a wide spectrum of disorders, including Leber's congenital amaurosis (4, 5), nephronophthisis (NPHP) (1), Joubert syndrome (JBTS) (2), and Meckel–Gruber syndrome (6, 7). JBTS is an inherited ciliopathy giving rise to NPHP with cerebellar vermis aplasia and retinal degeneration. Among patients with JBTS and a cerebello-oculo-renal phenotype, mutations in *CEP290* (*NPHP6*) are the most common genetic lesion (8). A unifying feature of JBTS-associated genes is the localization of their protein products within the primary cilium, and subsequent studies have focused on Wingless-Int (Wnt) and Hedgehog (Hh) signaling pathways disrupted in these ciliopathy conditions. Wnt signaling is a conserved developmental signaling pathway. In the canonical (β-catenin–dependent) Wnt pathway, Wnt ligand binds to a Frizzled receptor and produces, via stabilization and accumulation of β-catenin, nuclear transcription of Wnt target genes (9). β-catenin is a transcriptional coactivator of transcription factors in the Tcf/Lef family (10). Tcf/Lef proteins are dynamically expressed during development, and Wnt signaling controls many cellular processes, including cell proliferation and cell-fate determination (11). The Hh signaling pathway is required for normal organ development, patterning, and cell signaling and relies upon primary cilia to mediate its affects (12, 13). In the absence of Hh ligand, Patched (Ptch) blocks the activation of Smoothened (Smo), and transcription factors including Gli are processed into smaller repressor forms (GliR). However, in the presence of Hh binding to Ptch, Smo is released and leads to an increase in Gli in its activator form (GliA). Target-gene expression is thus finely balanced by the ratio of GliA and GliR. Ptch, Smo, and Gli proteins all localize to the primary cilium (14–16).

Although the primary cilium is vital for Hh signaling (13), there is conflicting evidence from mouse models as to the involvement of Wnt (17) and/or Hh (18) signaling in the cerebellar abnormalities of JBTS. Abnormal Wnt signaling is found in late stages of NPHP in kidneys from *Ahi1*$^{-/-}$ mutant mice (19); however, the activity of key signaling pathways remains to be assessed at the early stages of NPHP.

Results and Discussion

To investigate the molecular mechanisms underlying NPHP, we created a *Cep290* mutant mouse from mouse ES cells carrying an

Significance

The molecular mechanisms underlying the juvenile onset cystic kidney disease nephronophthisis, remain incompletely understood. Our mutant mouse model identifies abnormal Hedgehog signaling as the primary lesion in nephronophthisis, although currently the perceived knowledge is that aberrant wingless-int signaling is responsible. Primary kidney collecting duct cells isolated from mutant mice with nephronophthisis are morphologically and functionally rescued when Hedgehog signaling is stimulated. This finding was replicated in ex vivo cultured urine-derived renal epithelial cells from a patient with Joubert syndrome and nephronophthisis. Understanding the initial molecular mechanisms of nephronophthisis is a significant advancement of the wider field of ciliopathies and identifies Hedgehog signaling as a potential therapeutic target for these conditions.

Author contributions: P.E.T., N.L.S., C.G.M., and J.A.S. designed research; A.M.H., R.H.G., S.S., L.E., J.W., M.D., G.G.S., J.G.C., H.A., H.Y.K., P.E.T., N.L.S., C.G.M., and J.A.S. performed research; A.M.H., R.H.G., S.S., S.R., P.E.T., C.G.M., and J.A.S. analyzed data; and A.M.H., R.H.G., S.S., C.G.M., and J.A.S. wrote the paper.

The authors declare no conflict of interest.

This article is a PNAS Direct Submission.

[1]To whom correspondence may be addressed. E-mail: john.sayer@ncl.ac.uk or colin.miles@ncl.ac.uk.

This article contains supporting information online at www.pnas.org/lookup/suppl/doi:10.1073/pnas.1322373111/-/DCSupplemental.

insertion/truncation caused by insertion of a β-galactosidase gene trap vector. Chimeric male mice were bred with 129/Ola female mice to produce a wholly inbred strain in a single step. Breeding of the heterozygous *Cep290*$^{LacZ/+}$ mice produced homozygous animals that were fertile and viable beyond 12 mo of age (Fig. S1 *A–C*). The disruption was confirmed at both the mRNA and protein level in newborn kidneys where, despite some evidence of "read-through," there was an almost complete absence of protein detectable by Western blot (Fig. S2 *B* and *C*). All newborn animals were genotyped (n = 183). From the 129/Ola background, 21% were homozygous *Cep290*$^{LacZ/LacZ}$ animals, consistent with a normal Mendelian monogenic inheritance of a recessive allele (Fig. S1*D*). When backcrossed to the C57BL/6 strain, there was loss of a Mendelian distribution of alleles (Fig. S1*D*); most *Cep290*$^{LacZ/LacZ}$ animals died in utero, indicating strong genetic modifier effects consistent with the broad spectrum of phenotypes seen in patients carrying *CEP290* mutations and in the *pcy* (20) and *Tmem67* (21) mouse models. All subsequent studies were conducted on wholly 129/Ola purebred mice.

Cep290$^{LacZ/LacZ}$ mice exhibit a JBTS/ciliopathy phenotype, including retinal degeneration, cerebral abnormalities, and progressive cystic kidney disease, with evidence of polyuria and polydipsia, consistent with the human phenotype. Progressive retinal degeneration was evident from 4 wk of age, affecting the photoreceptor inner and outer segments cell layer and the outer nuclear layer (Fig. S3 *A–C*). There was no evidence of liver fibrosis in *Cep290*$^{LacZ/LacZ}$ animals (Fig. S3 *D–G*). MRI imaging of fixed tissues revealed hydrocephalus evident at 1 mo of age (Fig. S4*A*) although there was no evidence of a foliation defect within the cerebellum (Fig. S4*B*). Small cysts developed within the renal cortex of most but not all newborn *Cep290*$^{LacZ/LacZ}$ animals, becoming more prominent and more numerous at 2 wk of age, and persisting up to 1 y of age (Fig. 1 *A–D*). The cystic change is reminiscent of nephronophthisis. A quantification of cystic change over time confirmed kidney disease progression from newborn to 1 mo of age (Fig. S5*A*). Primary cilia were present on the epithelial cells of noncystic and cystic renal tubules of *Cep290*$^{LacZ/LacZ}$ animals but were significantly reduced in number (Fig. S5 *B* and *C*). Renal cysts were confirmed to be of collecting duct in origin,

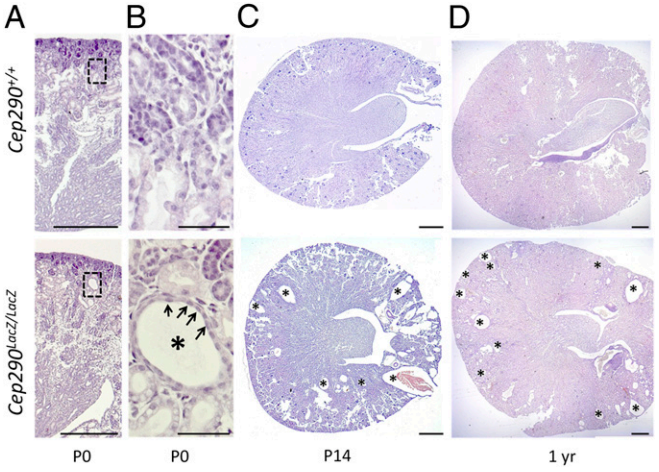

Fig. 1. *Cep290*$^{LacZ/LacZ}$ mice exhibit progressive renal collecting duct cystic disease. Representative kidney sections from wild-type *Cep290*$^{+/+}$ (*Upper*) and *Cep290*$^{LacZ/LacZ}$ mice (*Lower*) stained with hematoxylin/eosin. Microcysts are present in *Cep290*$^{LacZ/LacZ}$ kidneys from birth to 1 y (*A*, and magnified in *B*) at birth (P0), (*C*) 2 wk (P14), and (*D*) 1 y (1 yr) of age. The asterisk highlights collecting duct cysts, and arrows indicate the epithelial cell layer lining of a cyst. (Scale bars: *A*, 500 μm; *B*, 50 μm; *C* and *D*, 500 μm.)

expressing both the principal cell marker aquaporin-2 (22) and the intercalated cell marker Atp6V0A4 (23) (Fig. S5*D*).

Staining for β-galactosidase activity in *Cep290*$^{LacZ/+}$ animals indicated *Cep290* expression at the cortico-medullary boundary of the kidney, at the photoreceptor layer of the retina, and in the choroid plexus (Fig. S6). The strong expression seen in choroid plexus is consistent with our previous in situ hybridization study of human embryonic brain (24) and suggest that this ciliated structure may be involved in the cerebellar phenotypes associated with JBTS.

Because abnormal Wnt signaling has previously been reported in kidneys of *Ahi1*$^{-/-}$ mice with NPHP (19), we examined Wnt target Lef1 protein expression levels in whole-kidney lysates from newborn and 1-y-old mice. Western blotting for Lef1 demonstrated no change in Lef1 protein levels between *Cep290*$^{LacZ/LacZ}$ and wild-type littermate animals (Fig. 2*A*). Interestingly, in newborn kidney samples, Lef1 is seen as a doublet of two alternative spliced transcripts, which has previously been noted in embryonic murine brain (25). Tcf1 protein expression in newborn kidney was equal, again with alternative splicing evident as has been previously reported in human T cells (26). However, at 1 y of age, reduced levels of Tcf1 were clearly evident (Fig. 2*B*), suggesting that Wnt signaling is not dramatically changed during the early stages of kidney disease at the time of cystogenesis but is reduced at later stages of disease, possibly associated with kidney fibrosis. It is noteworthy that the majority of *Ahi1*$^{-/-}$ mutant mice die in utero on a C57BL/6 genetic background and that reduced Lef1 protein is observed in the kidneys of the survivors from 5 mo of age (19). Given that Ahi1 expression was linked to the Wnt–β-catenin signaling pathway (17, 19), we examined the expression of β-catenin within kidney tissue of *Cep290* mice. However, the expression levels of β-catenin were not different between *Cep290*$^{LacZ/LacZ}$ and wild-type littermate animals (Fig. 2*C*).

The primary cilium plays a critical role in Hh signaling, and many features of ciliopathy syndromes are associated with abnormal Hh signaling: for example, brain abnormalities in JBTS (18) and bone abnormalities in Ellis van Creveld syndrome (EVC) (27). To measure Hh activity in *Cep290*$^{LacZ/LacZ}$ mutant kidneys, we examined levels of the protein Gli3 activator and repressor isoforms in whole-kidney lysates from newborn mice (28, 29). Western blotting revealed a dramatic increase in the Gli3 repressor in *Cep290*$^{LacZ/LacZ}$ mutant kidneys (Fig. 2 *D* and *E*), similar to that seen in patients carrying *TCTN3* mutations (30) and the telencephalon of *Ftm* mice (31). Thus, *Cep290*$^{LacZ/LacZ}$ mice display an Hh deficiency that precedes a Wnt deficiency similar to that seen in adult *Ahi1*$^{-/-}$ mice. Determination of Gli1 expression in newborn mice also confirmed that an alteration in Hh signaling in *Cep290*$^{LacZ/LacZ}$ kidneys was evident (Fig. S5*E*).

The identification of abnormal Hh signaling at the earliest stages of NPHP raises the intriguing possibility that all ciliopathies may share a common etiology and that targeting the Hh signaling pathway may have therapeutic value for all manifestations of these conditions. To investigate the consequences of abnormal Hh signaling at the cellular level, we derived primary collecting duct cells, facilitated by introduction of the temperature-sensitive SV40-T-antigen by crossing with *H-2Kb-tsA58* mice (Fig. S1*E*). Collecting duct cells were isolated from *Cep290*$^{LacZ/LacZ}$ and wild-type mice using *Dolichos biflorus* Agglutinin (DBA) lectin selection. PCR was used to confirm the genotype of isolated cells, and Western blotting confirmed the reduction in Cep290 protein expression seen in mutant kidneys (Fig. S7 *A* and *B*). Both wild-type and mutant cells formed confluent epithelial monolayers consistent with a renal epithelium and also expressed markers of principal collecting duct cells, including the ENaC-alpha subunit and the mineralocorticoid receptor (Fig. S7*C*). Following serum starvation of primary collecting duct cells, primary cilia were seen in 56% of

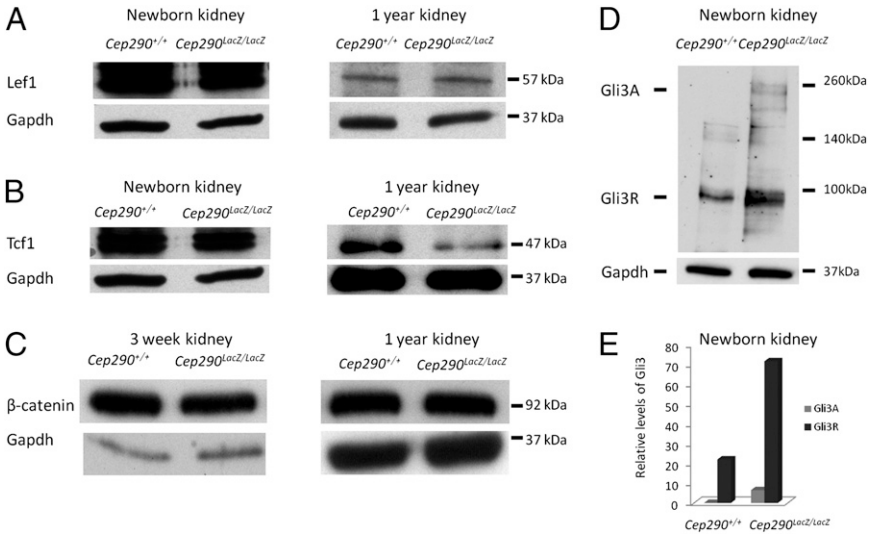

Fig. 2. Abnormal Hh but not Wnt signaling in *Cep290*$^{LacZ/LacZ}$ newborn kidneys. (*A*) Full-length isoform of Lef1 (~57 kDa) detected by Western blot of whole-kidney lysates from *Cep290*$^{+/+}$ and *Cep290*$^{LacZ/LacZ}$ littermates (newborn and 1 y of age), demonstrating no dramatic difference in levels of Lef1 protein expression between genotypes, relative to a Gapdh loading control. Band densitometry confirmed ratios of Lef1/Gapdh to be unchanged between *Cep290*$^{+/+}$ and *Cep290*$^{LacZ/LacZ}$ in newborn (4 vs.4.3) and 1 y kidney (0.19 vs. 0.21). (*B*) Tcf1 (~47 kDa) detected by Western blot of whole-kidney lysates from *Cep290*$^{+/+}$ and *Cep290*$^{LacZ/LacZ}$ littermates (newborn and 1 y of age) demonstrating normal levels of Tcf1 protein in newborn kidney (band densitometry ratios of Tcf1/Gapdh 2.3 vs. 2.5) but reduced levels of Tcf1 protein evident in *Cep290*$^{LacZ/LacZ}$ kidneys at 1 y of age. Band densitometry confirmed ratios of Tcf1/Gapdh to be 0.47 in *Cep290*$^{+/+}$ and 0.21 in *Cep290*$^{LacZ/LacZ}$. (*C*) β-catenin (~92 kDa) detected by Western blot of whole-kidney lysates from *Cep290*$^{+/+}$ and *Cep290*$^{LacZ/LacZ}$ littermates (3 wk and 1 y of age) demonstrating no difference in levels of β-catenin protein expression between genotypes, relative to a Gapdh loading control. (*D*) Gli3 detected by Western blot of whole-kidney lysates from *Cep290*$^{+/+}$ and *Cep290*$^{LacZ/LacZ}$ newborn littermates revealing elevated levels of the Gli3 repressor isoform (Gli3R) in *Cep290*$^{LacZ/LacZ}$ relative to Gapdh and (*E*) quantified using band densitometry. All Western blots were replicated at least three times using different biological samples.

wild-type cells (127 out of 227 cells) with a mean length of 3.5 μm whereas, in mutant cells, primary cilia were seen in only 4.5% of cells (13 out of 284 cells) and the cilia present were significantly shortened (mean length 2.3 μm) (Fig. S8 *D* and *E*).

Collecting duct cells characteristically self-polarize into spheroid structures when grown in 3D culture conditions; this system has been previously validated to model architectural defects in the context of renal ciliopathies such as NPHP (32, 33). Using this system, collecting duct cells from wild-type animals formed large spheroids with well-defined lumens (98%, 738/750 spheroids scored) at the equatorial plane of the spheroid revealing β-catenin lining the basolateral membranes, and primary cilia projecting into the lumen in 75% of the nuclei scored (n = 300) (Fig. 3*A*). *Cep290*$^{LacZ/LacZ}$ collecting duct cells, however, formed fewer spheroids, and those present were largely abnormal, with no lumen or a lumen with a diameter less than 10 μm (34%, 252/750 spheroids scored). Cilia formation was severely disrupted in these spheroids (Fig. 3*B*), with just 24% of nuclei at the equatorial plane being ciliated (n = 300). There was also a notable loss of junctional β-catenin. We postulate that reduced junctional β-catenin, as previously seen with *Nek8* siRNA targeting (34), is a consequence of the spheroid defects rather than its cause. The abnormal spheroids indicate that *Cep290*$^{LacZ/LacZ}$ collecting duct cells have an intrinsic deficiency that fundamentally affects their function, consistent with reduced collecting duct structure and function leading to NPHP.

Given that kidneys from *Cep290*$^{LacZ/LacZ}$ mice show evidence of reduced Hh signaling, we tested the effects of increasing Hh signaling in *Cep290*$^{LacZ/LacZ}$ collecting duct cells by addition of the Hh agonist purmorphamine to the spheroid 3D culture system. Purmorphamine treatment resulted in a dramatic improvement, such that *Cep290*$^{LacZ/LacZ}$ collecting duct cells organized into better spheroid structures with lumens over 10 μm (79%, 595/750 spheroids scored) and with an increased number of cilia (48%, 143/300 nuclei scored) and the formation of adherens junctions (Fig. 3 *C* and *F*). Thus, stimulation of Hh signaling can partially rescue the mutant phenotype, indicating that the mutant collecting duct cells are amenable to pharmacological manipulation and that they are not irreversibly damaged by the mutation. Furthermore, it is intriguing to note that purmorphamine can bypass the ciliary defects associated with *Cep290* mutation and restore the establishment of 3D architecture in the renal collecting duct while also moderately improving ciliogenesis. Cep290 is thought to play a gatekeeper role at the transition zone of the primary cilium (35) and to influence the entry and exit of proteins into the cilium. Another recently identified transition zone protein, CSPP1, has also been shown to be essential for ciliogenesis and interacts with other nephrocystin proteins (36). Hh signaling was noted to be downregulated in fibroblasts from patients with *CSPP1* mutations (37) presumably secondary to the loss of cilia. Our data point to the fact that Hh itself may be required for ciliogenesis, given that ciliogenesis in *Cep290*$^{LacZ/LacZ}$ spheroids is partially rescued. In reciprocal experiments, wild-type cells receiving HPI-4 treatment, an Hh pathway antagonist, cause a reduction in spheroid formation together with a loss of cilia (11% of cells remained ciliated, 31/300 nuclei scored) (Fig. 3 *D* and *G*).

We identified a JBTS patient with a typical cerebello-oculo-renal phenotype in whom molecular genetic diagnosis revealed compound heterozygous *CEP290* mutations of known pathogenicity (4, 38). Using ex vivo culture of urine-derived renal epithelial cells (URECs) from this patient we were able to replicate the spheroid and cilia defect seen in murine *Cep290*$^{LacZ/LacZ}$ collecting duct cells. In cultured URECs from the JBTS patient, spheroids were disorganized and smaller and had fewer cilia compared with wild type (Fig. 4 *A* and *B*). This defect could be partially rescued, with a significant recovery of spheroid architecture and cilia number using exogenous stimulation of Hh signaling with purmorphamine (Fig. 4 *C* and *D*).

Collectively, primary renal cells from a murine model were directly verified in cells from a patient showing that abnormal Hh signaling underlies juvenile NPHP and that pharmacological

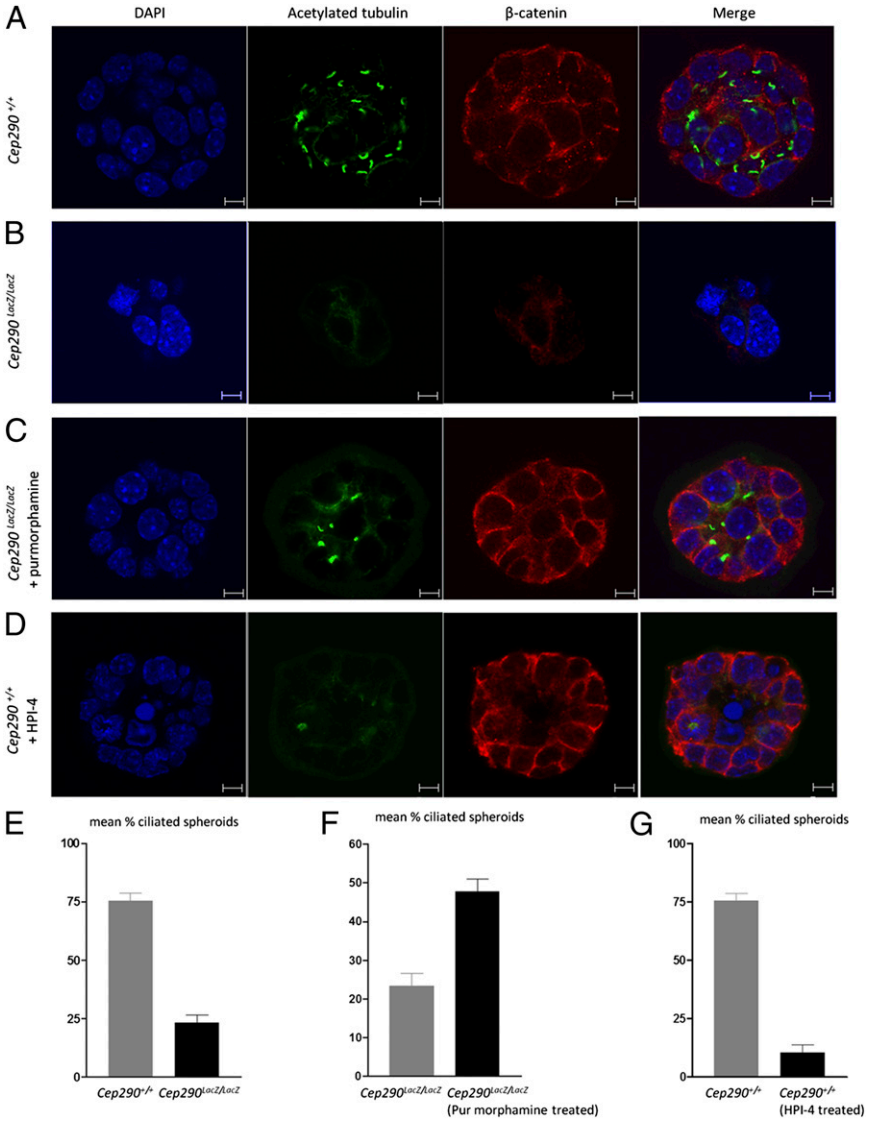

Fig. 3. *Cep290*$^{LacZ/LacZ}$ collecting duct cells are unable to form organized 3D spheroids ex vivo without exogenous stimulation of Hh signaling. Representative immunohistochemistry images (DAPI, blue; acetylated tubulin, green; β-catenin, red). (Scale bar: 5 μm.) (*A*) Normal 3D spheroid formation (observed in 98%, $n = 750$) from *Cep290*$^{+/+}$ collecting duct cells. (*B*) *Cep290*$^{LacZ/LacZ}$ collecting duct cells had a spheroid forming index of only 34% ($n = 1180$), with the remaining 66% containing fewer than 10 cells and/or no lumen. (*C*) Purmorphamine treatment restored 3D spheroid forming ability in 79% of *Cep290*$^{LacZ/LacZ}$ collecting duct cells ($n = 750$). (*D*) HPI-4 treatment of wild-type cells causes a reduction in spheroid formation (observed in 85%, $n = 600$). (*E*) Quantification of ciliogenesis reveals that 48-h serum starvation induced primary cilia in 75% of *Cep290*$^{+/+}$ spheroids, but only in 24% of *Cep290*$^{LacZ/LacZ}$ mutant cells. Data are shown as means ± SEM, $P = 0.0004$ determined by unpaired *t* test for each genotype. (*F*) Quantification of ciliogenesis reveals that *Cep290*$^{LacZ/LacZ}$ cells treated with 2 μM purmorphamine treatment for 72 h restored ciliogenesis from 24% (DMSO control) to 48%. Data are shown as means ± SEM; $P = 0.0063$ determined by unpaired *t* test for each genotype. (*G*) Quantification of ciliogenesis reveals that, when *Cep290*$^{+/+}$ cells were treated with 10 μM HPI-4 for 36 h, ciliogenesis was reduced from 75% (DMSO control) to 11%. Data are shown as means ± SEM, with $P = 0.0002$ determined by unpaired *t* test for each genotype.

treatment with Hh agonists represents a strong candidate for the development of novel therapies for NPHP and possibly other manifestations of the ciliopathies.

Methods

Mouse Genetics. All mouse work was performed under licenses granted from the Home Office (United Kingdom) in accordance with the guidelines and regulations for the care and use of laboratory animals outlined by the Animals (Scientific Procedures) Act 1986 and with the approval of the Newcastle University Ethical Review Committee. Using database searches accessed January 2, 2010 (www.ncbi.nlm.nih.gov/nucgss/), we identified a "gene trap" ES cell line (DU635568.1, Sanger Institute Gene Trap Library) in which the murine *Cep290* was disrupted at intron 23 to induce a hypomorphic mutation *Cep290*$^{LacZ/LacZ}$. The trap contains a β-galactosidase/neomycin reporter gene with a ribosomal reentry site followed by a poly(A) tail (Fig. S9 *A* and *B*). Genomic DNA PCR confirmed the correct insertion of the gene trap and was fine-mapped it to 3.308 kb downstream of exon 24. Genotyping was conducted using a combination of three oligonucleotide primers (F2, R2, and R5) (Fig. S9). The modified ES cells were injected into blastocysts to create chimeric mice. Male chimeras (129/Ola«C57/B6) were selected for mating with either 129/Ola or C57/B6 female mice to generate mice heterozygote for the *Cep290*$^{LacZ/LacZ}$ hypomorphic mutation on either pure 129/Ola or (C57/B6 × 129/Ola) F1 genetic backgrounds (Fig. S1). F1 heterozygotes were backcrossed with C57/F6 for six generations (C57/B6-F6) whereas a pure 129/Ola colony was established to eliminate any potential genetic background effects. Unless otherwise stated, all analyses were carried out on the inbred 129/Ola background.

Generation of "Immorto"mouse/*Cep290*$^{LacZ/LacZ}$ Cross. The *H-2Kb-tsA58* mouse line was crossed with the *Cep290*$^{LacZ/LacZ}$ mouse to generate double transgenic *Cep290*$^{LacZ/LacZ}$*::H-2Kb-tsA58*$^{+/-}$ and *Cep290*$^{+/+}$*::H-2Kb-tsA58*$^{+/-}$ mice (Fig. S1*D*). The transgene in these mice is usually dormant and can be activated only by culturing explanted cells at 33 °C. All transgenic mouse lines were maintained on the inbred C57Bl6/J background (Charles River). For genotyping, genomic DNA was extracted from mouse ear clips/cell pellets, and standard PCR was performed. Oligonucleotide primer sequences, including those used to confirm the "immorto" transgene (39), are shown in Fig. S9*C*.

Histological Examination of Tissues. Mouse tissues were dissected and fixed in 4% (wt/vol) paraformaldehyde (PFA) at 4 °C. Hematoxylin/eosin, Trichome Masson, and Sirius Red were used as per manufacturer's guidelines. All histology sections were visualized using an Olympus BX43F microscope.

Primary Collecting Duct Cell Culture. The *Cep290*$^{LacZ/LacZ}$*::H-2Kb-tsA58*$^{+/-}$ and *Cep290*$^{+/+}$*::H-2Kb-tsA58*$^{+/-}$ collecting duct cells were isolated from kidneys of 1-mo-old transgenic mice (Fig. S1*E*), resulting in "immortalized," primary, mutant, and wild-type collecting duct cells. Briefly, kidney samples were removed, sliced using a sterile scalpel, and digested with 0.5% collagenase type II (cat. no. 41H12763; Worthington Biochemical Corporation) in 0.1% BSA (cat. no. A2153; Sigma) for 30 min at 37 °C. This cell suspension digest was then mixed in 1:1 dilution of (cortical collecting duct) CCD media (40)

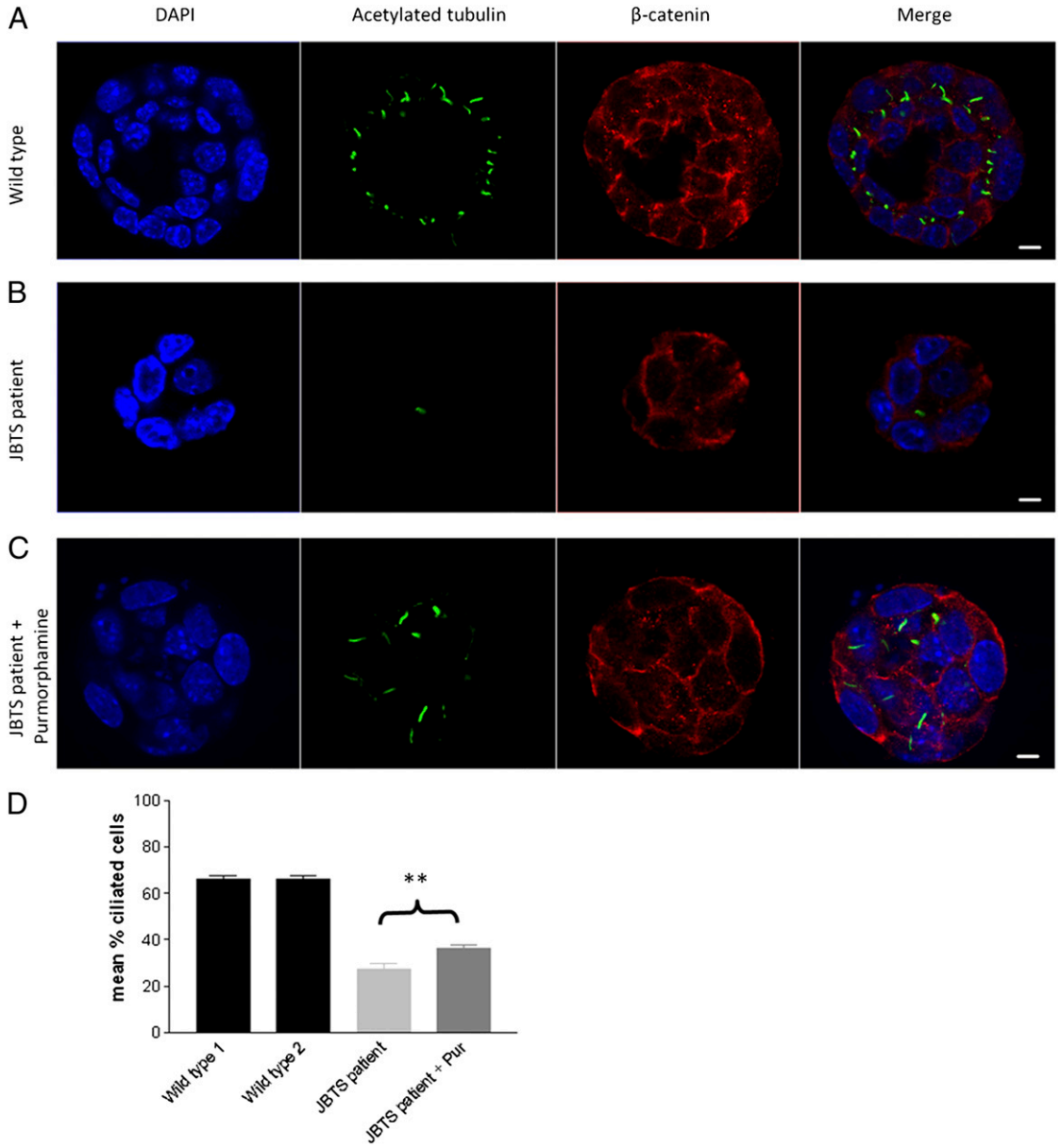

Fig. 4. JBTS urine-derived renal epithelial cells (URECs) are unable to form organized 3D spheroids ex vivo without exogenous stimulation of Hh signaling. Representative confocal immunocytochemistry images (DAPI, blue; acetylated tubulin, green; β-catenin, red). (Scale bar: 5 μm.) (*A*) Normal 3D spheroid formation from wild-type URECs. (*B*) JBTS patient URECs form abnormal spheroids that were smaller with fewer cilia. (*C*) Purmorphamine treatment partially restores 3D spheroid forming ability in JBTS URECs with improvement in both architecture and ciliary frequency. (*D*) Quantification of number of ciliated cells within 3D spheroids reveals primary cilia in 66% of cells from wild-type URECs ($n = 445$, wild-type 1; and $n = 503$, wild-type 2) but only in 27% of JBTS patient URECs ($n = 457$). JBTS patient URECs treated with 2 μM purmorphamine (Pur) for 68 h restored ciliogenesis to 36% ($n = 438$). Data are shown as means ± SEM, with $^{**}P = 0.0037$, unpaired *t* test.

plated onto six-well plates coated with 10 mg/mL *Dolichos biflorus* Agglutinin (DBA) (cat. no. L-2785; Sigma) (10 μg/mL in 0.1 M NaHC03) overnight at 33 °C. Unbound cells were removed with gentle washing in fresh culture media added, and cells were incubated at 33 °C in 5% CO_2. CCD media was used for cell culture as previously described (40). CCD media was changed every 48–72 h, and cultures were passaged when ∼70–80% confluent.

Western Blotting. Protein was extracted and lysed from frozen whole kidney tissue and cells and solubilized in a 4 M urea, 125 mM Tris (pH 6.8), 4% (wt/vol) SDS, 10% (vol/vol) glycerol, 5% (vol/vol) β-mercaptoethanol, and 0.02% bromophenol blue solution. Protein was extracted from collecting duct cells once they had reached confluency. Protein samples were heated to 95 °C for 5 min and then loaded onto 6–10% (wt/vol) polyacrylamide gels and run at 200 V for 1 h. Proteins were transferred to a nitrocellulose membrane at 350 mA for 1 h. The membranes were blocked in 5% (wt/vol) powdered milk in Tris-buffered saline and Tween 20 solution overnight at 4 °C and incubated with primary antibodies (goat anti-Gli3, 1:3,000, R&D Systems; rabbit anti-Lef1, 1:100, Cell Signaling; rabbit anti-Tcf1, 1:100, Cell Signaling; rabbit anti-Gli1 (V812), 1:500, Cell Signaling,; rabbit anti-β-catenin (6B3), 1:1,000, Cell Signaling) all for 2 h at room temperature and rabbit anti-Gapdh (1:10,000; Cell Signaling) for 1 h at room temperature. After washing in TBST, membranes were incubated in HRP-conjugated secondary antibodies (Dako and Jackson) and developed using ECL (Thermo). Band densitometry levels were performed using the Fiji software program (41).

Spheroid Growth Assay and Immunofluorescence. Ten thousand collecting duct cells from $Cep290^{LacZ/LacZ}$ or $Cep290^{LacZ/+}$ mice were mixed 1:1 with growth factor-depleted matrigel (BD Bioscience) in Labtech chamber slides. An identical protocol was followed for URECs, following their isolation and

culture, detailed in *SI Methods*. After polymerization for 40 min at 33 °C, warm medium was dripped over the matrix until just covered and cultured at 33 °C/5% CO_2. The cells formed spheroids with cleared lumens 3–4 d later. During the last 48 h, spheroids were cultured with medium with or without the presence of 2 μM purmorphamine. Medium was removed by pipetting, and the gels were washed three times for 10 min with warm PBS supplemented with calcium and magnesium. The gels were then fixed in fresh 4% (wt/vol) PFA for 30 min at room temperature. After washing three times in PBS after fixation, the cells were permeabilized for 15 min in gelatin dissolved in warm PBS (350 mg/50 mL) with 0.5% Triton X-100. Primary antibody (mouse anti-acetylated tubulin, 1:20,000, Sigma; and rabbit anti–β-catenin, 1:1,000, Cell Signaling) was diluted in permeabilization buffer and incubated overnight at 4 °C. After washing the spheroids three times for 30 min in permeabilization buffer, goat anti-mouse-Cy5, donkey anti-rabbit-TRITC, and goat anti-rat-FITC secondary antibodies (1:400; Invitrogen) were each diluted in permeabilization buffer and incubated in the dark for 4 h at room temperature. Spheroids were washed three times in permeabilization buffer for 10 min per wash and then incubated for 1 h with DAPI, before being washed an additional three times in PBS, and mounted in Fluoromount-G (Cell Lab; Beckman Coulter) overnight at room temperature in the dark. Images and *Z*-stacks were taken with a Zeiss LSM700 confocal microscope and 150 spheroids per condition were scored within 5 d of the experiment's end. GraphPad Prism was used to perform two-tailed *t* tests.

Purmorphamine and HPI-4 Treatment. Collecting duct cells and URECs were treated with 2 μM purmorphamine/DMSO treatment for 68–72 h (DMSO was used as a negative control), and 3D spheroids were analyzed using confocal microscopy. Collecting duct cells were treated with 10 μM HPI-4/DMSO treatment for 36 h (DMSO was used as a negative control), and the 3D spheroids were analyzed using confocal microscopy.

ACKNOWLEDGMENTS. We particularly thank the patient, his mother, and the control human subjects for their participation in this study. We thank Ive Logister and the Utrecht Cell Microscopy Center for technical assistance. A.M.H. is supported by the Northern Counties Kidney Research Fund and Kids Kidney Research. S.S. is a Kidney Research UK Clinical Training Fellow. R.H.G. and G.G.S. are supported by European Union/Framework Programme 7/2009 Consortium "SYSCILIA" Grant 241955. R.H.G. and H.Y.K. are supported by the Dutch Kidney Fundation "Kouncil" Consortium Grant CP11.18. H.A. is supported by the Anna-Liise Farquharson Kidney Cancer Research Fund, Princess Margaret Foundation. J.A.S. is supported by the Northern Counties Kidney Research Fund.

1. Sayer JA, et al. (2006) The centrosomal protein nephrocystin-6 is mutated in Joubert syndrome and activates transcription factor ATF4. *Nat Genet* 38(6):674–681.
2. Valente EM, et al.; International Joubert Syndrome Related Disorders Study Group (2006) Mutations in CEP290, which encodes a centrosomal protein, cause pleiotropic forms of Joubert syndrome. *Nat Genet* 38(6):623–625.
3. Andersen JS, et al. (2003) Proteomic characterization of the human centrosome by protein correlation profiling. *Nature* 426(6966):570–574.
4. Perrault I, et al. (2007) Spectrum of NPHP6/CEP290 mutations in Leber congenital amaurosis and delineation of the associated phenotype. *Hum Mutat* 28(4):416.
5. den Hollander AI, et al. (2006) Mutations in the CEP290 (NPHP6) gene are a frequent cause of Leber congenital amaurosis. *Am J Hum Genet* 79(3):556–561.
6. Travaglini L, et al.; International JSRD Study Group (2009) Expanding CEP290 mutational spectrum in ciliopathies. *Am J Med Genet A* 149A(10):2173–2180.
7. Baala L, et al. (2007) Pleiotropic effects of CEP290 (NPHP6) mutations extend to Meckel syndrome. *Am J Hum Genet* 81(1):170–179.
8. Valente EM, Brancati F, Boltshauser E, Dallapiccola B (2013) Clinical utility gene card for: Joubert Syndrome-update 2013. *Eur J Hum Genet*, 10.1038/ejhg.2013.10.
9. Logan CY, Nusse R (2004) The Wnt signaling pathway in development and disease. *Annu Rev Cell Dev Biol* 20:781–810.
10. Schuijers J, Mokry M, Hatzis P, Cuppen E, Clevers H (2014) Wnt-induced transcriptional activation is exclusively mediated by TCF/LEF. *EMBO J* 33(2):146–156.
11. Angers S, Moon RT (2009) Proximal events in Wnt signal transduction. *Nat Rev Mol Cell Biol* 10(7):468–477.
12. Wong SY, Reiter JF (2008) The primary cilium at the crossroads of mammalian hedgehog signaling. *Curr Top Dev Biol* 85:225–260.
13. Goetz SC, Anderson KV (2010) The primary cilium: A signalling centre during vertebrate development. *Nat Rev Genet* 11(5):331–344.
14. Rohatgi R, Milenkovic L, Scott MP (2007) Patched1 regulates hedgehog signaling at the primary cilium. *Science* 317(5836):372–376.
15. Milenkovic L, Scott MP, Rohatgi R (2009) Lateral transport of Smoothened from the plasma membrane to the membrane of the cilium. *J Cell Biol* 187(3):365–374.
16. Haycraft CJ, et al. (2005) Gli2 and Gli3 localize to cilia and require the intraflagellar transport protein polaris for processing and function. *PLoS Genet* 1(4):e53.
17. Lancaster MA, et al. (2011) Defective Wnt-dependent cerebellar midline fusion in a mouse model of Joubert syndrome. *Nat Med* 17(6):726–731.
18. Aguilar A, et al. (2012) Analysis of human samples reveals impaired SHH-dependent cerebellar development in Joubert syndrome/Meckel syndrome. *Proc Natl Acad Sci USA* 109(42):16951–16956.
19. Lancaster MA, et al. (2009) Impaired Wnt-beta-catenin signaling disrupts adult renal homeostasis and leads to cystic kidney ciliopathy. *Nat Med* 15(9):1046–1054.
20. Nagao S, et al. (1991) Strain difference in expression of the adult-type polycystic kidney disease gene, pcy, in the mouse. *Jikken Dobutsu* 40(1):45–53.
21. Abdelhamed ZA, et al. (2013) Variable expressivity of ciliopathy neurological phenotypes that encompass Meckel-Gruber syndrome and Joubert syndrome is caused by complex de-regulated ciliogenesis, Shh and Wnt signalling defects. *Hum Mol Genet* 22(7):1358–1372.
22. Nielsen S, DiGiovanni SR, Christensen EI, Knepper MA, Harris HW (1993) Cellular and subcellular immunolocalization of vasopressin-regulated water channel in rat kidney. *Proc Natl Acad Sci USA* 90(24):11663–11667.
23. Stehberger PA, et al. (2003) Localization and regulation of the ATP6V0A4 (a4) vacuolar H+-ATPase subunit defective in an inherited form of distal renal tubular acidosis. *J Am Soc Nephrol* 14(12):3027–3038.
24. Cheng YZ, et al. (2012) Investigating embryonic expression patterns and evolution of AHI1 and CEP290 genes, implicated in Joubert syndrome. *PLoS ONE* 7(9):e44975.
25. Nagalski A, et al. (2013) Postnatal isoform switch and protein localization of LEF1 and TCF7L2 transcription factors in cortical, thalamic, and mesencephalic regions of the adult mouse brain. *Brain Struct Funct* 218(6):1531–1549.
26. Willinger T, et al. (2006) Human naive CD8 T cells down-regulate expression of the WNT pathway transcription factors lymphoid enhancer binding factor 1 and transcription factor 7 (T cell factor-1) following antigen encounter in vitro and in vivo. *J Immunol* 176(3):1439–1446.
27. Ruiz-Perez VL, et al. (2007) Evc is a positive mediator of Ihh-regulated bone growth that localises at the base of chondrocyte cilia. *Development* 134(16):2903–2912.
28. Huangfu D, et al. (2003) Hedgehog signalling in the mouse requires intraflagellar transport proteins. *Nature* 426(6962):83–87.
29. Huangfu D, Anderson KV (2005) Cilia and Hedgehog responsiveness in the mouse. *Proc Natl Acad Sci USA* 102(32):11325–11330.
30. Thomas S, et al. (2012) TCTN3 mutations cause Mohr-Majewski syndrome. *Am J Hum Genet* 91(2):372–378.
31. Besse L, et al. (2011) Primary cilia control telencephalic patterning and morphogenesis via Gli3 proteolytic processing. *Development* 138(10):2079–2088.
32. Sang L, et al. (2011) Mapping the NPHP-JBTS-MKS protein network reveals ciliopathy disease genes and pathways. *Cell* 145(4):513–528.
33. Otto EA, et al. (2010) Candidate exome capture identifies mutation of SDCCAG8 as the cause of a retinal-renal ciliopathy. *Nat Genet* 42(10):840–850.
34. Choi HJ, et al. (2013) NEK8 links the ATR-regulated replication stress response and S phase CDK activity to renal ciliopathies. *Mol Cell* 51(4):423–439.
35. Betleja E, Cole DG (2010) Ciliary trafficking: CEP290 guards a gated community. *Curr Biol* 20(21):R928–R931.
36. Patzke S, et al. (2010) CSPP is a ciliary protein interacting with Nephrocystin 8 and required for cilia formation. *Mol Biol Cell* 21(15):2555–2567.
37. Shaheen R, et al. (2014) Mutations in CSPP1, encoding a core centrosomal protein, cause a range of ciliopathy phenotypes in humans. *Am J Hum Genet* 94(1):73–79.
38. Brancati F, et al.; International JSRD Study Group (2007) CEP290 mutations are frequently identified in the oculo-renal form of Joubert syndrome-related disorders. *Am J Hum Genet* 81(1):104–113.
39. Kern G, Flucher BE (2005) Localization of transgenes and genotyping of H-2kb-tsA58 transgenic mice. *Biotechniques* 38(1):38—42.
40. Bens M, et al. (1999) Corticosteroid-dependent sodium transport in a novel immortalized mouse collecting duct principal cell line. *J Am Soc Nephrol* 10(5):923–934.
41. Schindelin J, et al. (2012) Fiji: An open-source platform for biological-image analysis. *Nat Methods* 9(7):676–682.